Electronic structures of oxygen adsorption on {110} nickel-rich pentlandite ($Fe_4Ni_5S_8$) mineral surface

P.P Mkhonto[1], H.R Chauke[1] and P.E Ngoepe[1]

[1]Materials Modelling Centre, University of Limpopo, Private Bag x1106, Sovenga, 0727, South Africa

E-mail: peace.mkhonto@gmail.com

Abstract. Pentlandite $(Co,Fe,Ni)_9S_8$ is the most abundant iron-nickel sulphide ore containing mineral and has a wide range of applications in industries. The mineral is of commercial importance and can be extracted using floatation processes; one of the processes is by oxidation. This process plays a significant role in forming air bubbles that float the pentlandite mineral. Despite reports that oxidation tend to depress the sulphide minerals, it however, increases the pulp potential during flotation. The present study investigate the clean and oxidised nickel-rich {110} pentlandite surface using *ab-initio* density functional theory (DFT). The Bader analysis have been used to evaluate clean and oxidised surface and suggests that Fe and Ni have 3+ and 2+ (clean) and 4+ and 3+ (oxidised) oxidation state, respectively. Furthermore, when oxygen is adsorbed on the (fcc-hollow site or on Fe-top site) and on Ni-top site, it was found that the surface oxidises as Fe-O-Fe and Ni-O-O, respectively. Oxidation had also shown preferential of iron and we noted a charge transfer from the metals to the oxygen molecule. We also observed that the oxygen (O1) coordinated to the Fe/Ni increases the states of σ_s and π_p bonding orbitals with no π_p* antibonding orbital present. Furthermore, the oxygen (O2) coordinated to O1 occupies the π_p* antibonding orbital. The σ_p* antibonding peak is observed to move closer to the Fermi energy, where on Fe-top site adsorption the peak reside just above the Fermi energy while on Ni-top site adsorption is half occupied.

1. Introduction

The oxidation of pentlandite, naturally and during floatation is an important process to understand extraction of mineral ore. As there is a growing demand for nickel [1], pentlandite, in particular $(Fe, Ni)_9S_8$ is a principal source of nickel [2]. Pentlandite mineral occurs as intergrowth or in solid solution with pyrrhotite [3] and this makes extraction of mineral difficult. The separation of minerals can be achieved by the use of organic collectors which form important role in rendering the mineral hydrophobic [4].

According to literature, floatation is made easy by creating the rising current that acts like 'hot-air balloons' as such providing the necessary buoyancy to carry selected minerals to the pulp surface. Floatation is the process by which air is bubbled through the slag in a floatation cell. The bubbled air usually oxidises the minerals and also create air bubbles [5]. The alteration, in particular the oxidation both in ore deposits and during the extraction, is an important process used during extraction of mineral ore [3]. In this regard it is of paramount importance to investigate the oxidation process. This will provides information on the chemistry of pentlandite surfaces that may be applicable to the separation of pentlandite mineral. In this study we report on DFT

computational investigation of the adsorption strength, bonding behavior, charge transfer and interaction of oxygen molecule with the {110} surface of nickel-rich pentlandite ($Fe_4Ni_5S_8$) mineral.

2. Computational methodology

In order to investigate the surface-O_2 reaction on nickel-rich pentlandite mineral we perform *ab initio* quantum-mechanical density functional theory [6; 7] calculations and analyze the density of states, Bader charges and charge density difference. Bader analysis is necessary for calculating and assigning electronic charges on individual atoms within the system. This is based upon a grid of charge density values where only steepest ascent trajectories confined to the grid points are used to identify the Bader regions [8].

We use the plane-wave (PW) pseudopotential method with Perdew-Burke-Ernzerhof (PBE) exchange-correlation functional [9] in spin-polarized condition, using VASP code [10]. A {110} surface slab composed of four layers of atoms separated by a vacuum slab of 20 Å was used to mimic the interaction of the adsorbate (O2) with the repeating upper slab. The ultrasoft pseudopotential is used with a plane-wave basis set, truncated at a kinetic energy of 400 eV since this was found to be sufficient to converge the total energy of the system. Brillouin zone integrations are performed on a grid of 5x5x1 k-points. This is chosen according to the scheme proposed by Monkhorst and Pack [11]. We use the Methfessel-Paxton smearing of σ = 0.2 eV. Different termination were sampled and only the less reactive (low surface energy) for {110} surfaces were considered. The surface stabilities for different termination are determined by their surface energy, calculated using equation 1:

$$E_{surface} = \left(\frac{1}{2A}\right)[E_{slab} - (n_{slab})(E_{bulk})] \quad (1)$$

where E_{slab} is the total energy of the cell containing the surface slab, n_{slab} is the number of atoms in the slab, E_{bulk} is the total energy per atom of the bulk and A is the surface area. A low positive value of $E_{surface}$ indicates stability of the surface termination. During adsorption the bottom two layers are kept frozen and the top four layers are allowed to interact with the oxygen molecule. The strength of interaction of the surface with the adsorbate is shown by the adsorption energy, calculated by equation 2:

$$E_{adsorption} = \left(\frac{1}{n}\right)[E_{slab} - (E_{system} + nE_{adsorbate})] \quad (2)$$

where E_{system} is the energy of the surface slab with adsorbate, E_{slab} is the energy of the surface slab as above, n is the number of adsorbate adsorbed on the surface and $E_{adsorbate}$ is the energy of the isolated adsorbate molecule. A negative value shows a strong interaction between the adsorbate and the surface, whereas a positive value reveals the opposite.

3. Results and discussion

The nickel-rich pentlandite ($Fe_4Ni_5S_8$) {110} surface is shown in figure 1, and the designated atoms as indicated. The surface was cleaved from the optimised bulk pentlandite structure with space group of *Fm-3m* (225) [12].

Table 1. Calculated surface energy (eV/Å^2) and adsorption energies (eV) of oxygen molecule adsorbed on {110} nickel-rich pentlandite mineral surface metals.

Surface	Surface energy	Adsorption energies		
{110}	$E_{(surface)}$	Fcc-hollow	Ni-top	Fe-top
	0.061	-1.891	-0.040	-1.902

In order to describe the adsorption of oxygen on the surface, we consider three distinct adsorption trajectories as shown in figure 1(f). The three adsorptions labelled as fcc-hollow, Fe-top and Ni-top. Their calculated surface and adsorption energies are given in table 1. The adsorption strength of oxygen molecule on the surface is found to be stronger on the Fe atoms. We observed that O_2 adsorption on the Fe-top and fcc-hollow site forms bridging with the iron atoms (Fe-O-Fe), and their adsorption energy is slightly more exothermic on Fe-top than fcc-hollow site. It clearly suggests that energy (0.011 eV) is lost in the chemisorption process of fcc-hollow site. Now, considering the adsorption on Ni-top, we observed formation of a superoxo bonding giving rise to adsorption energy of -0.040 eV. It is evident that the adsorption energy of Fe is more spontaneous than on Ni, this suggests the preferential oxidation of Fe. The oxidation behaviour is in line with that reported by Merape *et al*. [13], where the oxygen molecule prefers the iron.

Figure 1(a) and (b) show the un-relaxed and relaxed surfaces, respectively. We observed that after relaxation, the slab changes from four layers (figure 1(d)) to six layers (figure 1(e)), where layer1 relaxes into three layers as shown in figure 1(e). In order to predict the bonding behavior and charge state of the surface, we consider the spin-polarized density of states (DOS) in figure 1(c) and Bader analysis in table 2. Note that the DOS are plotted only for the top most metals (i.e. Fe and Ni) atoms. The DOS shows that this material has a metallic characteristic since there is no band gap observed at the Fermi energy (E_F). The PDOS of Ni atoms show only one sharp peak at the VB and less contribution at E_F, while the PDOS of Fe has broader peaks around E_F. More importantly, we note that the Fermi energy cut the top of Fe d-orbital (high states at E_F).

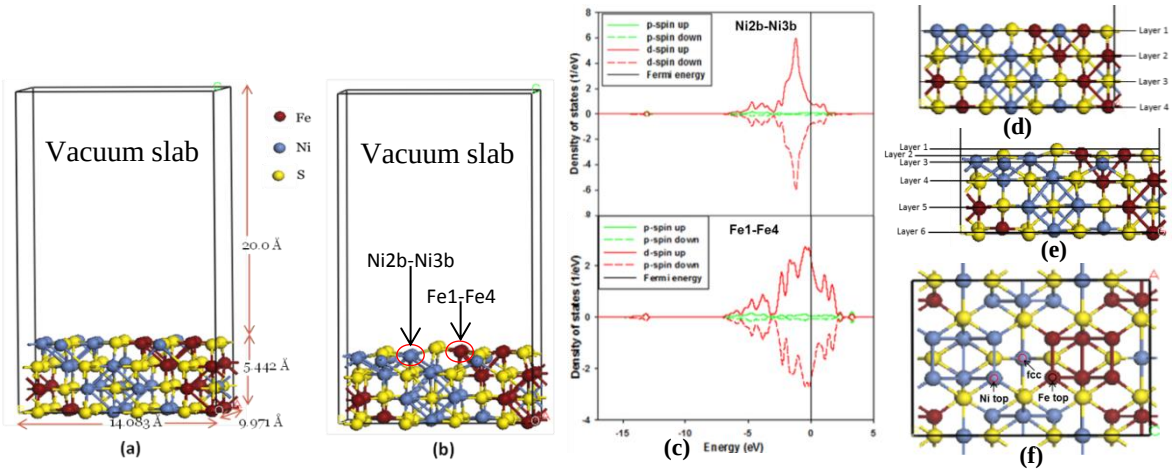

Figure 1: The {110} surface (a) un-relaxed and (b) relaxed stable termination surface, (c) PDOS of the top most clean Fe/Ni atoms, (d) number of layers on the relaxed surface and (e) the three different adsorption geometries investigated: fcc-hollow, Fe-top and Ni-top.

Table 2: The Bader analysis for Fe-O_2 and Ni-O_2 on {110} surfaces: Atom, Bader charge and oxidation state.

Surface	Atom	Clean surface		Fe-top adsorption		Ni-top adsorption	
		Bader charge (e^-)	Oxidation state	Bader charge (e^-)	Oxidation state	Bader charge (e^-)	Oxidation state
{110}	O1	-	-	6.483	-0.48e	6.253	-0.25e
	O2	-	-	6.150	-0.15e	6.118	-0.12e
	Fe1	7.575	+0.43e	7.281	+0.72e	-	-
	Fe4	7.505	+0.51e	7.292	+0.71e	-	-
	Ni2b	9.593	+0.41e	-	-	9.361	+0.64e

The clean iron atoms are observed to have different oxidation states (charges) suggesting that the iron atoms are not charge ordered and there is alternation of the charges. This suggests that the presence of nickel atoms at the octahedral position breaks the charge symmetry of the iron atoms to a small degree, such that the iron with $Fe^{0.43+}$ has 0.08 electrons less than the $Fe^{0.51+}$. Such observations of the charge symmetry breakage have been observed on doping of bulk FeS with Ni [14]. The Bader charges for the clean surface suggested oxidation states of Fe^{3+} and Ni^{2+} (table 2). From covalent materials, by analogy it can be deduced that there is a high level of covalent nature predicted for the Ni-S and Fe-S bonds in $Fe_4Ni_5S_8$ pentlandite.

From the calculated Bader analysis of adsorbed system we noted that oxygen (O2) accepts less charges compared to the surface bonding oxygen (O1) (table 2). The charge loss on Ni and Fe atoms increases their oxidation states, suggesting a transformation from Ni^{2+} to Ni^{3+} and Fe^{3+} to Fe^{4+} oxidation states. The oxidation state of Ni^{3+} only occurs with fluoride and oxide [15], thus suggest a Ni^{3+}.

Table 3. The relaxed bond lengths (*R*, in Å), bond angles (θ, in deg.). The theoretical/ Experimental values are shown in parenthesis for comparison.

	Oxidation		
Bonds	Fcc-hollow site	Fe-top site	Ni-top site
R(O1-O2)	1.316	1.316	1.284 (1.284) [16]
R(Fe1-O1)	1.818 (1.880) [17]	1.815 (1.880) [17]	-
R(Fe4-O1)	1.818 (1.880) [17]	1.817 (1.880) [17]	-
R(Ni2b-O1)	-	-	1.801 (1.728) [16]
θ(Fe1-O1-Fe4)	84.68˚ (81.9) [18]	84.96˚ (81.9) [18]	-
θ(Ni2b-O1-O2)	-	-	128.78˚ (125.3) [16]

An interesting observation is that the bond length of Fe1-O1 is shorter compared to Fe4-O1, suggesting that Fe1 losses more charges. These charge transfer is also complimented by the charge density difference (figure 2(f and g)) where we note that a positive electronic cloud that accepts electrons is on oxygen molecule while the negative electronic cloud that donate is on the Ni/Fe atoms. In figure 2(d and e), the relaxed system shows a superoxide or superoxo bonding of oxygen molecule on both Ni and Fe atoms. Superoxo or superoxide is a compound that contains the superoxide anion with the chemical formula O_2^-. Superoxide anion is particularly important as the product of the one-electron reduction of dioxygen O_2, which occurs widely in nature [19]. The bond distances found (table 3), are in agreement with previous studies and confirmed formation of a superoxo bonding. The cylindrical shape on the oxygen (O2) atom also suggests a superoxo bonding.

Now we present and discuss the spin-polarized density of states (DOS) of oxidised surface (figures 2(a) and (b)). The charge density difference between the oxidised surface system and the clean surface plus the oxygen molecule are visualised using the VESTA software [20]. In order to confirm the charge transfer during adsorption we compute the Bader analysis (table 2). These calculated properties are crucial since they depict the nature of bonding for the adsorbate on the surface as it is not easy to clearly define the bond order from structural analysis. Note that here we only show the DOS and Bader analysis for adsorption on Fe-top and Ni-top, since the fcc-hollow site adsorption showed similar behaviour as the adsorption on Fe-top.

Figure 2(a) and (b) show the DOS for the two adsorption sites, i.e. Fe-top and Ni-top sites. Now, we consider the Fe-top adsorption, the DOS clearly shows that the Fe d-orbital transfer electrons to both bonding and antibonding of the O_2 orbitals, in particular we observe that the LUMO π_p^* antibonding orbital is occupied below the E_F. The Fe PDOS show sharp d-orbital peaks below the E_F compared to the clean surface. Furthermore, the peaks above the E_F merge to form

one peak that has very small splitting peaks. This suggests that electrons are being donated to the oxygen atoms.

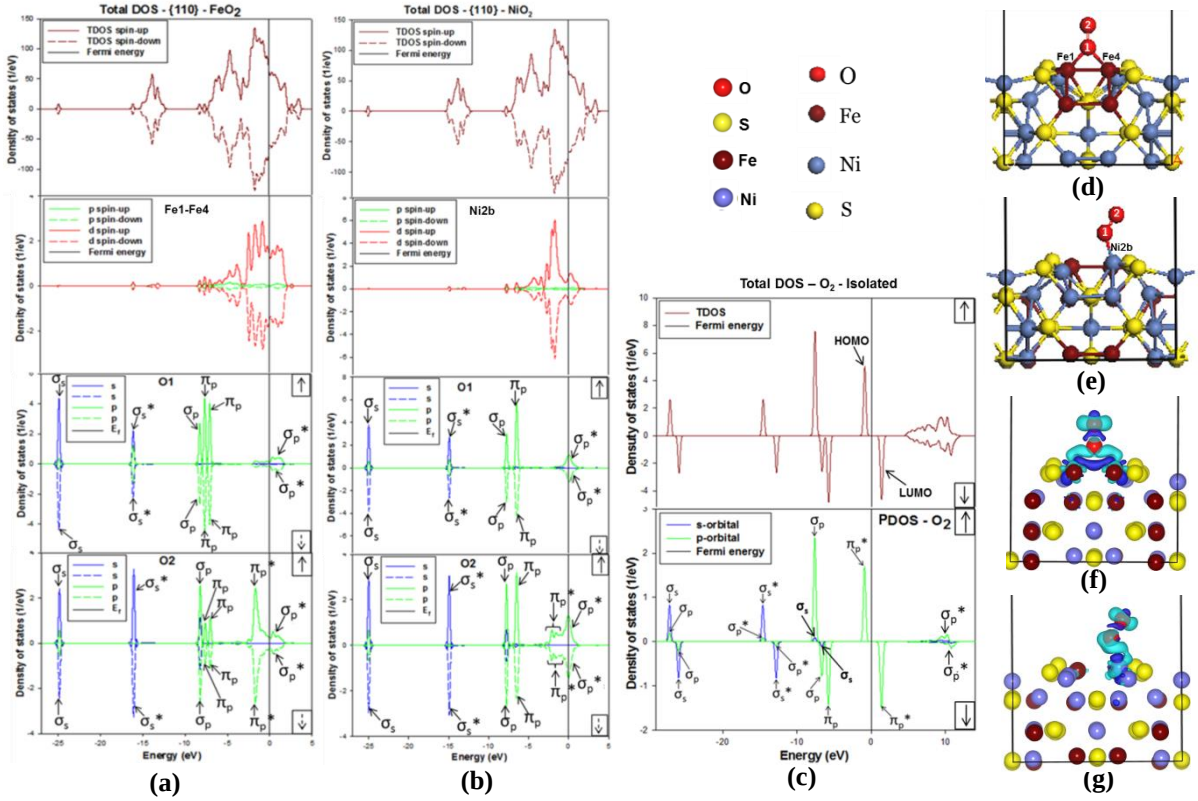

Figure 2: The total density of states (tDOS) and PDOS: (a) adsorption on Fe-top site, (b) adsorption on Ni-top site. Side view of relaxed surface with oxygen molecule: (c) energy levels of the valence orbitals of isolated O_2 molecule, (d) Fe-top site ad sorption and (e) Ni-top site adsorption. The sketch of isosurface charge density difference: showing electron transfer between surface metals (Ni/Fe) atoms and oxygen atoms on the surface: (f) Fe-top site (isosurface level = 0.004 eÅ^{-3}) and (g) Ni-top site (isosurface level = 0.003 eÅ^{-3}). Cyan represents positive electronic clouds which accept electrons and blue stands for negative electronic clouds which donate electrons.

The PDOS of O_2 shows that σ_s and π_p bonding orbitals and π_p* antibonding orbitals accepts electrons during bonding of the O_2 on the Fe. It is worth noting that O1 is the bridging (bonding) oxygen atom and we observed that it occupies more of the σ_s and π_p bonding orbitals since an increased state are noted with no π_p* antibonding present below the E_F (figure 2(a) and (b)). The O2 is noted to have the π_p* antibonding orbitals occupied just below the E_F, suggesting that electrons prefer the outer most shell. Interestingly, we note that the σ_p bonding orbitals on both O1 and O2 is similar to that of the isolated O_2. Furthermore, we observe that the σ_p* antibonding orbital moves closer and reside just above the E_F and mix with the d-orbital antibonding.

For Ni-top adsorption (figure 2(b)), the PDOS clearly shows that the sharp d-orbitals peak split into two peaks. Moreover, we noted a formation of a small peak just above the E_F. However, the peak is not completely shifted/formed above the E_F, suggesting that the σ_p* orbital is not fully occupied and as such show hybridisation of the antibonding d-orbitals and σ_p* orbital. The PDOS of O_2 molecule (figure 2(b)) of Ni-top shows similar behaviour as Fe-top, however, the difference in this case (Ni-top) is that the π_p* antibonding orbital has broad peaks, thus reducing their states

height. Moreover, we noted that the σ_p* orbital on is half occupied at the Fermi energy and merges with the π_p* orbital.

4. Conclusions

The adsorption energy and bonding nature of oxygen molecule on the {110} surface for flotation purpose was investigated using DFT. We observed that the oxidation favoured the formation of superoxo on Ni-top site and a bridging on iron on Fe-top and fcc-hollow site. Furthermore, we observed a preferential oxidation of iron on fcc-hollow site adsorption. The DOS revealed that the oxygen (O2) not attached to the metal surface has the π_p* orbital occupied, while the bonding orbitals on O1 have increased states compared to the antibonding orbitals. Interestingly, Bader analysis revealed the amount of charge transferred and those accepted; in which case we noted that O1 accept more charges than O2. The loss of charges on the metals suggested transformation from Ni^{2+} to Ni^{3+} and from Fe^{3+} to Fe^{4+} oxidation states. This study showed how oxygen reacts with iron/nickel naturally and during flotation which is an aspect that may be useful in the floatation of pentlandite mineral.

Acknowledgements

The calculations were performed at the Materials Modelling Centre (MMC), University of Limpopo. We acknowledge the Centre for High Performance Computing (CHPC) for computing resources. Thanks to the South African Mineral to Metals Research Institute (SAMMRI) for financial support.

References

[1] Ngobeni WA and Hangone G 2013 The effect of using sodium di-methyl-dithiocarbamate as a co-collector with xanthates in the froth flotation of pentlandite containing ore from Nkomati mine in South Africa. *Miner. Eng.* **54** 94–99.

[2] Borodaev Yu, Bryzgalov S I A, Mozgova N N and Uspenskaya T 2007 Pentlandite and Co-Enriched Pentlandite as Characteristic Minerals of Modern Hydrothermal Sulfide Mounds Hosted by Serpentinized Ultramafic Rocks (Mid-Atlantic Ridge) *Vestnik Moskovsk Universiteta Geologiya* **62** 85–97.

[3] Rajamani V and Prewitt C T 1973 Crystal chemistry of natural pentlandites *Can. Mineral.* **12** 178–187.

[4] (n.d.). Retrieved January 13 2013 from http://www.chem.mtu.edu/chem_eng/faculty/kawatra/Flotation_Fundamentals.pdf

[5] (n.d.). Retrieved october 20 2012 from www.jmeech.mining.ubc.ca/MINE290/Froth%20Flotation.pdf

[6] Hohenberg P and Kohn W 1965 Inhomogeneous electron gas *Phys. Rev.* B **136** 864–71.

[7] Kohn W and Sham L J 1965 Self-consistent equations including exchange and correlation effects. *Phys. Rev.* **140** 1133–38.

[8] Bader R F W 1994 *Atoms in Molecules: A Quantum Theory* London: Oxford University Press.

[9] Heyd J, Scuseria G E and Ernzerhof M 2003 *J. Chem. Phys.* **118** 8207.

[10] Kresse G and FurthermÜller J 1996 Efficient iterative schemes for ab-initio total-energy calculations using a plane-wave basis set *Phys. Rev. B* , **54** 11169–186.

[11] Monkhorst H F and Park J D 1976 Special points for Brillouin-Zone integrations. *Phys. Rev.* B **13** 5188–92.

[12] Geller S 1962 *Acta. Cryst.* 1195.

[13] Merape G 2010 *Fundamental Electrochemical Behaviour of Pentlandite* Pretoria: University of Pretoria.

[14] Devey A J and de Leeuw N H 2009 *Computer Modelling Studies of Mackinawite, Greigite and Cubic FeS* University College London Department of Chemistry.

[15] Housecroft C E and Shape A G 2008 *Inorganic chemistry (3rd ed)* Prentice Hall.

[16] Gutsev G L, Rao B K and Jena P 2000 Systematic Study of Oxo, Peroxo, and Superoxo Isomers of 3d-Metal Dioxides and Their Anions. *J. Phys. Chem. A* **104** 11961–971.
[17] Pearce C I, Henderson C M B, Telling N D, Pattrick R A D, Vaughan D J, Charnock J M, Arenholz E, Tuna F, Coker V S and Van der Laan G 2010 Iron site occupancies in magnetite-ulvöspinel solid solution: A new Approach using XMCD *Am. Mineral.* 1–37.
[18] Wang L 2000 Photodetachment photoelectron spectroscopy of transition oxide species. **10** 854–957.
[19] Sawyer D T (n.d.) Superoxide Chemistry McGraw-Hill.
[20] Momma K and Izumi F 2013 October VESTA: a Three-Dimensional Visualization System for Electronic and Structural Analysis, *National Museum of Nature and Science 4-1-1 Amakubo, Tsukuba Ibaraki 305-0005 Japan and National Institute for Materials Science 1-2-1 Senge, Tsukuba Ibaraki 305-0047 Japan* 1-172.